

# Comparison of ion sites and diffusion paths in glasses obtained by molecular dynamics simulations and bond valence analysis

Christian Müller,<sup>1</sup> Egbert Zienicke,<sup>1</sup> Stefan Adams,<sup>2</sup> Junko Habasaki,<sup>3</sup> and Philipp Maass<sup>1\*</sup>

<sup>1</sup>*Institut für Physik, Technische Universität Ilmenau, 98684 Ilmenau, Germany*

<sup>2</sup>*Department of Materials Science and Engineering,*

*National University of Singapore, Singapore 117576*

<sup>3</sup>*Tokyo Institute of Technology, 4259 Nagatsuta-cho, Yokohama 226-8502, Japan*

(Dated: June 21, 2006)

Based on molecular dynamics simulations of a lithium metasilicate glass we study the potential of bond valence sum calculations to identify sites and diffusion pathways of mobile Li ions in a glassy silicate network. We find that the bond valence method is not well suitable to locate the sites, but allows one to estimate the number of sites. Spatial regions of the glass determined as accessible for the Li ions by the bond valence method can capture up to 90% of the diffusion path. These regions however entail a significant fraction that does not belong to the diffusion path. Because of this low specificity, care must be taken to determine the diffusive motion of particles in amorphous systems based on the bond valence method. The best identification of the diffusion path is achieved by using a modified valence mismatch in the BV analysis that takes into account that a Li ion favors equal partial valences to the neighboring oxygen ions. Using this modified valence mismatch it is possible to replace hard geometric constraints formerly applied in the BV method. Further investigations are necessary to better understand the relation between the complex structure of the host network and the ionic diffusion paths.

PACS numbers: 66.30.Dn, 66.30.Hs

## I. INTRODUCTION

On a coarse grained time scale, ionic conduction in glasses is commonly described by a thermally activated jump motion of the mobile ions in an irregular host framework formed by a network former ( $\text{SiO}_2$ ,  $\text{B}_2\text{O}_3$ , ...). Regions of long residence times in the network are associated with sites, and rare events, where ions move between neighboring sites, are associated with jumps. The problem how to identify and characterize sites and diffusion paths in such non-crystalline materials poses a challenging task of current research activities. Its solution can be expected to play a key role in approaching a more quantitative understanding of ion transport properties in glasses.<sup>1</sup> Methods developed in this field should be useful also for the description of thermally activated transport processes in other disordered systems.

In recent molecular dynamics simulations of modified network glasses<sup>2,3,4,5,6,7,8</sup> sites were identified based on the number density  $\rho(\mathbf{x})$  of the mobile ions. In some of these works, the sites constitute those spatial regions, where  $\rho(\mathbf{x})$  exceeds a certain threshold  $\rho_*$ . The threshold value was specified by requiring the number of these regions to be maximal (for details of the procedure and the question which of these regions are identified with sites, see ref. 2 and the analysis in Sec. III). The sites form during the cooling process in the highly viscous melt<sup>9</sup> and are stable on the time scale of the main structural rearrangements of the network, which, below the glass transition temperature, is much larger than the time scale needed for the mobile ions to reach the long-time diffusion regime. For the systems investigated,<sup>2,3,4,5,6,7,8</sup> the number of sites exceeds the number of ions by 6-12% only,

suggesting that a vacancy mediated hopping dynamics<sup>10</sup> should be considered in a coarse grained description.<sup>11,12</sup> Due to the interaction effects the ionic motion can be strongly cooperative in such situations, as reported by one of the authors,<sup>3,8</sup> and also in ref. 13.

Although the method of determining the local number density in MD simulations was by following the trajectories of the mobile ions and by registering their occupation times in small cells (over sufficiently long time periods), it should be noted that  $\rho(\mathbf{x})$  can be viewed as an equilibrium quantity with respect to configurations belonging to the metastable attraction basin of the free energy reached after the cooling process. This means, that in the absence of aging effects, which involve transitions between different basins,  $\rho(\mathbf{x})$  can in principle be determined independently of the ion dynamics.

Experimentally, a measurement of the local number density of mobile ions with respect to the host structure of the network forming ions is currently not possible. Unlike in crystals, it is already difficult to obtain a reliable representation of the framework structure. The most successful procedure to date is to use x-ray and neutron diffraction data as input for a reverse Monte Carlo modeling.<sup>14</sup> Structures obtained in this way are in agreement with the static structure factors and they fulfill certain constraints imposed by chemical requirements. Recently this structural modeling has been combined with bond valence (BV) sum calculations in order to identify diffusion paths for mobile ions in network glasses.<sup>15,16,17,18</sup> However, while for various crystalline systems it could be demonstrated that both sites and pathways predicted by the BV method match the results from detailed anharmonic crystal structure

analyses,<sup>19,20,21,22</sup> the potential of the BV method for predicting diffusion pathways or sites in amorphous systems needs to be clarified.

Since ionic transport pathways in glasses cannot be directly inferred from experiment, we test the BV method in this work by MD simulations. The interaction potentials used in our MD simulations were derived from ab initio Hartree-Fock self-consistent calculations and were checked to keep the crystal structure stable under constant pressure conditions.<sup>23</sup> This is a severe test of the quality of the potential parameters. Many properties of ion conducting glasses, as e.g. structural information obtained from scattering experiments, vibrational spectra, values for ionic diffusion and various thermodynamic properties are successfully reproduced by the MD model. Using the MD simulations as a reference to test the BV method, we nevertheless have to bear in mind that the underlying Hamiltonian for the interactions between the ions and the way of vitrifying in the MD simulations (e.g. the high cooling rates) may not give a fully accurate representation of all properties of the real experimental system. In any case, even if the representation with respect to the sites and conduction pathways is not perfect, one should expect that the BV method is still applicable, since the MD model itself presents a valid physical system. For the model system, however, the optimal parameters used in the BV analysis could possibly be different from those applied to the corresponding real glass (cf. Sec. IV).

Our results show that the BV paths entail the sites of the mobile ions in the MD simulations. The BV method yields a reasonable estimate of the number of sites for the mobile ions, but is not well suitable for locating the sites within the pathways. In order to evaluate the potential of the BV method with respect to diffusion pathways, the latter have to be specified from MD simulations. Such specification can be done based on  $\rho(\mathbf{x})$ , by using the percolation threshold  $\rho_{\text{perc}}$  for attributing the regions with  $\rho(\mathbf{x}) > \rho_{\text{perc}}$  to the diffusion path. We will show that the BV path reaches a sensitivity up to 56%, i.e. it covers up to 56% of this diffusion path, and, conversely, the specificity lie in the range 50-60%, i.e. 50-60% of the BV path belong to the diffusion path. A variant of the BV method recently developed by one of the authors,<sup>24</sup> allows us, by introducing a penalty function for unfavorable asymmetric bonding situations, to achieve a sensitivity up to 90% and a specificity between 30-60%.

The paper is organized as follows. After a description of the MD simulations in Sec. II, we perform an identification of the ion sites in Sec. III following the procedure suggested in ref. 2. We include a discussion of the role of the grid spacing used in this procedure and suggest an alternative criterion to finally assign the regions with  $\rho(\mathbf{x}) > \rho_*$  to sites. The diffusion path is determined from a percolation analysis. In Sec. IV we perform a BV analysis based on time-averaged network configurations obtained from the MD simulations and evaluate in Sec. V the potential of the BV method for identifying

TABLE I: Potential parameters for the MD simulations (cf. eq. (1)).

Ion	$z$	$a$ [Å]	$b$ [Å]	$c$ [Å <sup>3</sup> √kJ/mol]
Li <sup>+</sup>	0.87	1.0155	0.07321	22.24
Si <sup>4+</sup>	2.40	0.8688	0.03285	47.43
O <sup>2-</sup>	-1.38	2.0474	0.17566	143.98
$f_0 = 4.186 \text{ kJ}\text{Å}^{-1}\text{mol}^{-1} \quad r_c = 1.3 \text{ Å}$				

ion sites and the diffusion path by comparing the results with those obtained in Sec. III. Finally, we give in Sec. VI a summary of the results and an outlook to further research.

## II. MOLECULAR DYNAMICS SIMULATIONS

We perform MD simulations of a Li<sub>2</sub>SiO<sub>3</sub> glass in the NVE ensemble at a temperature of 700 K with periodic boundary conditions. Newton's equations are solved using the Verlet algorithm with time step  $\Delta t = 1$  fs. The computational domain is a cubic box of side length  $L = 16.68 \text{ Å}$  filled with 144 lithium, 72 silicon and 216 oxygen ions. The box size was determined by performing simulations in the NPT ensemble at atmospheric pressure. It corresponds to material densities that match the experimental ones within 5% of error.

Pair potentials of Gilbert-Ida type<sup>25,26</sup> describe the interactions between the species:

$$U_{ij}(r) = \frac{e^2}{4\pi\epsilon_0} \frac{z_i z_j}{r} + f_0(b_i + b_j) \exp\left(\frac{a_i + a_j - r}{b_i + b_j}\right) - \frac{c_i c_j}{r^6}, \quad (1)$$

where the parameters listed in table I have been optimized<sup>23</sup> and shown to give good agreement with experimental data.<sup>23,27,28,29</sup> The first term in eq. (1) is the Coulomb interaction with effective charge numbers  $z_i$  for Li, Si and O. The long-range Coulomb interaction with the image charges in the periodically continued copies of the simulation box is taken into account by standard Ewald summation. A Born-Meyer type potential  $A_{ij} \exp(-r/\lambda_{ij})$  in the second term of eq. (1) takes into account the repulsive short-range interactions, where the parameters  $a_i$  and  $b_j$  appearing in (1) decompose  $A_{ij}$  and  $\lambda_{ij}$  into values assigned to the interacting species. The last term in eq. (1) is a dispersive interaction and present only for interactions between oxygen ions with distance larger than  $r_c = 1.3 \text{ Å}$ .<sup>30</sup>

We cooled down the system in the NVT ensemble using a velocity scaling to reach the final temperature of  $T = 700 \text{ K}$  and subsequently equilibrated the system in the NVE ensemble. For the analysis of the results we performed a simulation run over 40 ns. Figure 1a shows

the pair correlation functions for Li-Li, Li-Si and Li-O that allow us to check if the minimal distances between pairs of ions used in the BV analysis (2.48 Å for Li-Si and 1.7 Å for Li-O, see below) fit to the potential model (1). The time-dependent mean square displacement of Li, O and Si ions is displayed in Figure 1b. The mean square displacement of the Li ions becomes normal diffusive at time scales larger than several hundred picoseconds, while that of the Si and O ions practically stays constant over the whole time interval. On the time scale of 2 ns, for which most of the calculations for the determination of sites and diffusion paths are carried out, aging effects of the network structure can be neglected.

### III. IDENTIFICATION OF ION SITES AND THE DIFFUSION PATH

During their motion the Li ions explore only parts of the host network. To identify the regions encountered by the Li ions and their favorable sites, the local number density  $\rho(\mathbf{x})$  of Li ions is calculated. Dependent on a threshold value  $\rho_{\text{th}}$ , we define a path  $\mathcal{P}(\rho_{\text{th}}) = \{\mathbf{x} | \rho(\mathbf{x}) > \rho_{\text{th}}\}$  as the region with  $\rho(\mathbf{x}) > \rho_{\text{th}}$ , and perform a subsequent cluster analysis of the paths in dependence of  $\rho_{\text{th}}$ . To determine  $\rho(\mathbf{x})$  the simulation box is subdivided into a grid of cubic cells with spacing  $\Delta$  and the time  $t_i$  is registered, where it is occupied by a Li ion. The average density  $\rho_i \simeq \rho(\mathbf{x}_i)$  in cell  $i$  is then calculated as  $\rho_i = (t_i/t_{\text{sim}})\Delta^{-3}$ , where  $t_{\text{sim}}$  is the total simulation time.

In order to identify regions of high probability of occupation we determine clusters of connected (face sharing) cells  $i$  with  $\rho_i > \rho_{\text{th}}$  by the Hoshen-Kopelman algorithm.<sup>31</sup> Figure 2 shows the number of clusters  $N_{\text{cl}}(\rho_{\text{th}})$  in dependence of  $\rho_{\text{th}}$  for three grid spacings  $\Delta$ . All three curves have the same shape: Starting from large  $\rho_{\text{th}}$ ,  $N_{\text{cl}}(\rho_{\text{th}})$  increases with decreasing  $\rho_{\text{th}}$ , since an increasing number of local maxima in  $\rho(\mathbf{x})$  is identified. The strong dependence on the grid spacing at large  $\rho_{\text{th}}$  shows that the local maxima in  $\rho(\mathbf{x})$  are sharp. For larger  $\Delta$ , less local maxima and consequently less clusters are found, since the average density  $\rho_i$  in a cell containing a sharp local maximum of  $\rho(\mathbf{x})$  becomes smaller and can fall below  $\rho_{\text{th}}$ . As long as  $\Delta$  is much smaller than the typical distance between the local maxima one expects that with decreasing  $\rho_{\text{th}}$  eventually all local maxima are resolved. This is indeed the case, as can be seen from the fact that the curves for different  $\Delta$  pass the same maximum at  $N_{\text{cl}}^{\text{max}} \simeq 165$ . By further decreasing  $\rho_{\text{th}}$  different clusters merge and  $N_{\text{cl}}(\rho_{\text{th}})$  decreases.

The discussion makes clear that there exists a plateau  $N_{\text{cl}}(\rho_{\text{th}}) = N_{\text{cl}}^{\text{max}}$  in the range  $\rho_{\text{min}} < \rho_{\text{th}} < \rho_{\text{max}}$ , which depends on the grid spacing (while the value  $N_{\text{cl}}^{\text{max}}$  is not affected for sufficiently small  $\Delta$ ). Above  $\rho_{\text{max}}$  some of the local maxima in  $\rho(\mathbf{x})$  are not resolved and below  $\rho_{\text{min}}$  clusters coalesce (which does not exclude that some of the  $N_{\text{cl}}^{\text{max}}$  clusters contain more than one local maximum of

$\rho(\mathbf{x})$ ). To identify clusters with possible Li sites one could choose any value of  $\rho_{\text{th}}$  in the threshold range  $\rho_{\text{min}} < \rho_{\text{th}} < \rho_{\text{max}}$ . This would not change the identity of the possible sites but their size. In order to cover as much volume as possible we use  $\rho_{\star} \equiv \rho_{\text{min}} \simeq 0.56 \text{ Å}^{-3}$  for a unique definition of the clusters, which are candidates for sites (strictly speaking, one should use the value  $\rho_{\text{min}}$  in the limit  $\Delta \rightarrow 0$ , since  $\rho_{\text{min}}$  depends weakly on  $\Delta$ ). The subsequent analysis is carried out for the smallest spacing  $\Delta = 0.139$ .

Next we study properties of the clusters with respect to their assignment to sites. To this end we determine the volume  $V_{\text{cl}} = n_{\text{cells}}\Delta^3$  of the clusters and the mean number density  $\rho_{\text{cl}} = \sum_{i \in \text{cl}} \rho_i / n_{\text{cells}}$  of Li ions on them, and number the clusters in order of increasing  $\rho_{\text{cl}}$ .  $n_{\text{cells}}$  denotes the number of cells in the corresponding cluster. Figures 3a,b,c show  $\rho_{\text{cl}}$ ,  $V_{\text{cl}}$ , and the occupation probability  $t_{\text{cl}}/t_{\text{sim}} = \sum_{i \in \text{cl}} t_i / t_{\text{sim}} = \rho_{\text{cl}} n_{\text{cells}} \Delta^3$  for the numbered clusters. The nearly constant increase of the density is interrupted by a jump after cluster number 17. Also the other two quantities show a strong increase in this region. The first clusters are very small and have very low occupation times. After the jump, the volume and the occupation time lie on a main branch between 0.6 and 0.35 Å<sup>3</sup> for the volume and between 50 and 90% of the ratio of occupation time to simulation time. In between there are some outliers with less volume or less occupation time, but above the values of the first 17 clusters. With these results one faces two problems: (i) Summing up the occupation probability of all clusters, one finds that the total occupation probability  $\sum_{\text{cl}} t_{\text{cl}}/t_{\text{sim}}$  of all clusters is 70% only. (ii) According to the behavior of all three shown quantities — very small occupation probability, volume and occupation time — the first clusters before the jump do not fit to the physical picture which one has of a site.

Problem (i) can be solved as follows. The criterion  $\rho(\mathbf{x}) > \rho_{\star}$  cuts off the outer fringe of a site, which is visited only a short time by a Li ion, but dynamically can be assigned to the site, since a Li ion in general returns to the cluster after entering its fringe. The clusters thus can be viewed to form the core of the sites. Problem (ii) is more subtle. As suggested in ref. 2, one can require that a cluster should only be assigned to a site if the mean occupation of Li ions on it exceeds a certain threshold. However, there can exist sites, which are visited only rarely but which still conform to the requirement of a sufficiently large ratio between the residence time of a Li ion on the site and the time for its transition to a neighboring site.

We therefore use a new criterion for the assignment of the clusters to sites by associating two times with each cluster, the total residence time  $t_{\text{res}}$  and the total hopping time  $t_{\text{hop}}$  to any of its neighbors. The hopping time is calculated as follows: When a Li ion leaves a cluster and enters a new one without returning, it performs a transition between two clusters. The hopping time then is the time interval between the departure from the initial cluster

ter and the arrival at the target cluster. Summing over all transitions starting from a given cluster, one obtains the total hopping time from this cluster. The time interval between the entrance of a Li ion into a cluster and the onset of its transition to another cluster yields the residence time, and by taking the sum over all events we obtain  $t_{\text{res}}$ .<sup>32</sup> Note that according to this definition the residence time includes events, where a Li ion leaves the cluster but returns to it before entering another cluster.<sup>33</sup>

Figure 4a shows  $t_{\text{res}}$  and  $t_{\text{hop}}$  for the numbered clusters. While  $t_{\text{hop}}$  fluctuates from cluster to cluster but never exceeds one tenth (0.2 ns) of the simulation time (2 ns),  $t_{\text{res}}$  shows a more smooth variation with the cluster number as a consequence of a strong correlation to  $\rho_{\text{cl}}$ . In particular, clusters with the smallest  $\rho_{\text{cl}}$  correspond to the one with lowest  $t_{\text{res}}$ . The total residence probability  $\sum_{\text{cl}} t_{\text{res}}/t_{\text{sim}}$  of the Li ions on the clusters is now 98%, which confirms that the problem with the low total occupation probability  $\sum_{\text{cl}} t_{\text{cl}}/t_{\text{sim}}$  is resolved by taking into account the fringes of the clusters.

In order for a cluster to be assigned to a site, we now use the criterion that its residence time  $t_{\text{res}}$  should be at least one order of magnitude larger than its total hopping time  $t_{\text{hop}}$ ,<sup>34</sup>

$$\frac{t_{\text{res}}}{t_{\text{hop}}} > 10. \quad (2)$$

Figure 4b shows  $t_{\text{res}}/t_{\text{hop}}$  for the numbered clusters. Most clusters fulfill condition (2), which demonstrates that the Li motion can be represented by a hopping dynamics on a coarse grained time scale larger than  $t_{\text{hop}}$ . Only 17 fail to satisfy condition (2), and almost all of those have small numbers corresponding to low  $\rho_{\text{cl}}$ . This shows that there is hardly any difference here between a criterion based on a threshold number density and (2). Accordingly, the sites are determined essentially by the equilibrium quantity  $\rho(\mathbf{x})$  (in the metastable basin after the cooling when disregarding slow non-equilibrium aging processes of the network structure). In total, we find 148 sites, which are only 2.8% more than the number of Li ions. This fraction of empty sites is slightly lower than that found in earlier studies<sup>2,3,4</sup> and supports the picture of an ion hopping with a small number of vacancies. Different from the usual situation in crystalline systems in thermal equilibrium, the concentration of vacancies here should be considered as a result of the freezing process and will not change significantly with temperature below the glass transition.

After having identified the sites, we determine the diffusion path. To this end we evaluate the percolation threshold<sup>35</sup>  $\rho_{\text{perc}}$  and the corresponding subset  $\mathcal{P}_{\text{perc}} = \mathcal{P}(\rho_{\text{perc}})$  of cells, on which the Li ions can diffuse across the system. We find  $\rho_{\text{perc}} = 0.030 \text{ \AA}^{-3}$ , where  $\mathcal{P}(\rho_{\text{perc}})$  covers 7.0% of the volume of the system (cf. table III). Confining the Li motion to exactly the critical percolation path at  $\rho = \rho_{\text{perc}}$  would yield anomalous subdiffusion. However, in our case the percolation threshold is not sharp due to the finite system size and the number

density of the Li ions takes into account only the mean occupation probabilities of the ions but not their thermal fluctuations. Even more important, these issues are not of particular relevance here, since we are interested in the spatial overlap with the BV paths (see Sec. IV). With respect to this overlap the criticality plays no decisive role (since connectivity properties are not important for the overlap).

#### IV. BOND VALENCE ANALYSIS

The development of the bond valence approach has its origin in the search of correlations between bond lengths, chemical valence and binding energies for the chemical bond,<sup>36</sup> and has been widely applied to crystals with covalent and ionic bonds. The possibility to approximately describe both types of bonding using the same formalism makes it particularly useful for inorganic compounds with partially covalent bonds. A review of the BV method is given in refs. 20,21. We describe the method here in connection with our application, which is the determination of sites and diffusion paths for the Li ions based on the knowledge of the Si-O network structure. For a Li ion to be accommodated in some region, its valence should be close to its “natural values”, and additional constraints for its coordination number and minimal distance to neighboring ions are to be satisfied (see below).

According to Pauling,<sup>36</sup> each bond in a structure induces, due to its polarity, bond valences of opposite sign (partial charges in units of the elementary charge  $e$ ) at the two atoms that it connects. In an equilibrated structure, the bond valences of an ion induced by neighboring counterions should add to its ideal value (i.e. +1 for a Li ion). Since the effective overlap of electronic orbitals typically decreases exponentially with distance of the atomic nuclei, the partial valence  $s_j(\mathbf{x})$  of a Li ion at position  $\mathbf{x}$  induced by an oxygen ion  $j$  at position  $\mathbf{x}_j$  is determined by<sup>37</sup>

$$s_j(\mathbf{x}) = \exp \left[ \frac{r_0 - |\mathbf{x} - \mathbf{x}_j|}{\xi} \right], \quad (3)$$

where  $r_0$  is the ideal bond length and  $\xi$  is the so-called softness parameter that determines how fast the bond valence varies with distance. The total valence  $V(\mathbf{x})$  of a Li ion is computed as the sum of the bond valences  $s_j(\mathbf{x})$ :

$$V(\mathbf{x}) = \sum_j s_j(\mathbf{x}) = \sum_j \exp \left[ \frac{r_0 - |\mathbf{x} - \mathbf{x}_j|}{\xi} \right]. \quad (4)$$

Because of the exponential decay with distance the sum can be extended over all oxygen ions in the computational domain (taking into account the minimum image convention for periodic boundary conditions). The decomposition (4) into bond valences allows one also to associate a coordination number  $C(\mathbf{x})$  of a Li number at

TABLE II: Parameters used in the BV analysis.

$\xi$ [Å]	$r_0$ [Å]	$s_{\min}$	$C_{\min}$	$C_{\max}$	$R_{\text{LiO}}$ [Å]	$R_{\text{LiSi}}$ [Å]	$\bar{V}$
0.516	1.17096	0.04	4	6	1.70	2.48	0.814

position  $\mathbf{x}$ . This is defined by the number of oxygen ions contributing  $s_j(\mathbf{x})$  exceeding a threshold  $s_{\min}$ ,

$$C(\mathbf{x}) = \sum_j \theta(s_j(\mathbf{x}) - s_{\min}), \quad (5)$$

where  $\theta(\cdot)$  is the Heaviside jump function ( $\theta(x) = 1$  for  $x > 0$  and zero else).<sup>18</sup> Here we choose  $s_{\min}$  as suggested by Brown.<sup>20</sup> The BV parameters  $r_0$ , and  $\xi$  are derived from a variety of crystalline phases,<sup>38,39</sup> and are given in table II.

Figure 5a shows the histogram of valences of the 144 Li ions for an instantaneous equilibrated configuration. While in a crystalline structure the Li ions  $i$  at their equilibrium positions  $\mathbf{x}_i$  have valences  $V_i = V(\mathbf{x}_i)$  close to the ideal value  $V_{\text{id}} = 1$ , we find a mean value  $\bar{V}_{\text{inst.}} = 0.821$  significantly smaller than  $V_{\text{id}}$  in the (instantaneous) amorphous glass structure. An apparent under-bonding of the Li ions with average BV sums of ca. 0.9 has been found also in the BV analysis of RMC models obtained from scattering data<sup>18</sup> and can be traced back to the non-crystalline structure of the glass. Since in the MD simulation the cooling rates are much larger than in experiments, the deviation from the ideal bonding situation in a crystal at thermal equilibrium is even larger.

With respect to the application of the BV analysis to structural models obtained from RMC simulations, one should take into account that the information provided by x-ray and neutron diffraction data corresponds to time-averaged positions of the network forming ions. This is due to the fact that the time for obtaining an evaluable signal is orders of magnitudes larger than a typical vibrational time. This means that a (non-unique) network configuration obtained in RMC modeling is a representative for a time-averaged density. We thus determined the mean positions of oxygen and silicon ions in a time interval of 2 ns and calculated the valences of Li ions with respect to these mean positions. For a Li ion placed at the centers  $\mathbf{x}_i$  of the cells  $i$  described in the previous section III (spacing  $\Delta = 0.139$  Å), the valences  $V_i = V(\mathbf{x}_i)$  were calculated. Taking into account the probability of occupation  $\rho(\mathbf{x}_i)\Delta^3$  of the cells, we then determined the probability density  $p(V)$  of valences shown in Fig. 5b. Its mean  $\bar{V} = 0.814$  is even slightly smaller than that for the instantaneous configuration, confirming that the ideal value  $V_{\text{id}} = 1$  is not the preferred one in the MD simulation of an amorphous glass structure. A small asymmetry is seen in  $p(V)$  with a steeper decrease from its maximum on the side of large valences  $V$ . This reflects the asymmetry of the two-body interaction potentials of Li with O ions, where small distances corresponding to the repulsive part yield larger

valences according to eq. (3), while large distances corresponding to the attractive part yield smaller valences. Since the asymmetry is not pronounced, the mean value  $\bar{V}$  is close to the value where  $p(V)$  attains its maximum.

In the following we analyze the data with respect to the time-averaged network structure and consider  $\bar{V}$  as the “optimal value” of the bond valence sum. The valence mismatch of a Li ion at position  $\mathbf{x}$  is then given by

$$d(\mathbf{x}) = |V(\mathbf{x}) - \bar{V}|. \quad (6)$$

The mean valence mismatch 12% calculated from  $p(V)$  in Fig. 5b is significantly larger than in crystalline structures (where typical values are less than 5%).

Following the BV method, a position  $\mathbf{x}$  is accessible for a Li ion if the following conditions are fulfilled:

- (i) The distances of the Li cation to silicon cations must exceed a minimum distance

$$\min_j \{|\mathbf{x} - \mathbf{x}_j^{\text{Si}}|\} > R_{\text{LiSi}}, \quad (7)$$

$R_{\text{LiSi}} = 2.48$  Å is chosen to be equal to (or a little less than) the sum of the radii of the two ions in agreement with the correlation hole of the pair correlation shown in Fig. 1a.

- (ii) According to the “equal valence rule”<sup>20</sup> among the conceivable states with matching BV sum, the one with more symmetric bonds is energetically preferable. The simplest way of excluding that a matching BV sum is achieved by an unphysical strong asymmetric coordination shell is to define a minimum acceptable bond distance,

$$\min_j \{|\mathbf{x} - \mathbf{x}_j^{\text{O}}|\} > R_{\text{LiO}}. \quad (8)$$

A value of  $R_{\text{LiO}} = 1.7$  Å is in agreement with the correlation hole in Fig. 1a and restricts a partial Li-O bond valence to values smaller than 0.36.

- (iii) The coordination number has to lie between a minimal and maximal value,

$$C_{\min} \leq C(\mathbf{x}) \leq C_{\max}, \quad (9)$$

where  $C_{\min} = 4$  and  $C_{\max} = 6$ . This condition has previously been assumed for sites only.<sup>18</sup>

- (iv) The valence mismatch must be smaller than a threshold value  $d_{\text{th}}$ ,

$$d(\mathbf{x}) = |V(\mathbf{x}) - \bar{V}| < d_{\text{th}}. \quad (10)$$

As an alternative to the three conditions (ii-iv) one can use just one condition (v), which is a modification of (iv). It takes into account that a Li ion is better accommodated to the local network environment at position  $\mathbf{x}$  if the valences  $s_j(\mathbf{x})$  are more symmetrically distributed among the neighboring oxygen ions. The effect can be

TABLE III: Volume fractions (%) of the various subsets specifying sites and diffusions paths.

$\mathcal{P}_{\text{sites}}$	$\mathcal{P}_{\text{perc}}$	$\mathcal{P}_{\text{ex}}^{\text{BV}}$	$\mathcal{P}_{\text{cn}}^{\text{BV}}$	$\mathcal{P}_{\text{ex+cn}}^{\text{BV}}$
1.4	7.0	10.0	83.0	8.3

described by defining an “ideal partial valence”  $s_{\text{id}}$  by  $C_{\text{min}}s_{\text{id}} = V_{\text{id}}$ ,<sup>18,24</sup> corresponding to a Li ion that, when symmetrically connected to  $C_{\text{min}}$  oxygen ions, has the ideal total valence  $V_{\text{id}}$ . The deviation from the symmetric situation is quantified by the penalty function

$$p(\mathbf{x}) = \sqrt{\sum_j \left( \frac{s_j(\mathbf{x})}{s_{\text{id}}} - 1 \right)^{2\mu}}, \quad (11)$$

where the sum is taken over all oxygen ions and we choose  $\mu = 3$ . A modified valence then is defined by  $d'(\mathbf{x}) = d(\mathbf{x}) + p(\mathbf{x})$  and we require:

- (v) The modified valence mismatch must be smaller than a threshold value  $d_{\text{th}}$ ,

$$d'(\mathbf{x}) = |V(\mathbf{x}) - \bar{V}| + p(\mathbf{x}) < d_{\text{th}}. \quad (12)$$

When applying eq. (12) instead of eq. (10) conditions (ii) and (iii) are no longer needed. As a consequence, instead of the four parameters  $R_{\text{LiO}}$ ,  $C_{\text{min}}$ ,  $C_{\text{max}}$ , and  $s_{\text{min}}$  the parameter  $\mu$  enters the calculation.

To perform the BV analysis, the computational domain is divided into a grid of cells with spacing  $\Delta$  analogous to the procedure used in sec. III ( $\Delta = 0.139$  Å). A cell is accessible if a Li ion placed at its center fulfills the requirements (i-iv), or (i,v) in the modified BV method.<sup>40</sup> The union of such cells is the BV path  $\mathcal{P}_{\text{BV}}(d_{\text{th}})$  (for conditions (i-iv)) or the BV path  $\mathcal{P}'_{\text{BV}}(d_{\text{th}})$

## V. COMPARISON OF ION SITES AND DIFFUSION PATHS

We first clarify the relevance of the purely geometric constraints (i,ii) in combination with the coordination number condition (iii), without taking into account the bond valence condition (iv). Accordingly we distinguish between the subsets defined by applying the constraints separately:  $\mathcal{P}_{\text{ex}}^{\text{BV}}$  is the subset given by the geometric exclusions (i,ii), while  $\mathcal{P}_{\text{cn}}^{\text{BV}}$  refers to the condition imposed solely on the coordination number (iii). The subset defined by the combined conditions (i-iii) is denoted as  $\mathcal{P}_{\text{ex+cn}}^{\text{BV}}$ .

The geometric conditions (i,ii) already limit the fraction of available space for the mobile ions to 10% for the time-averaged network structure, see table III. By contrast, constraint (iii) alone for  $s_{\text{min}} = 0.04$  is a weak condition, which would allow a Li ion to occupy 83% of

TABLE IV: Comparison of the subsets determined by the BV analysis according to criteria (i-iii) with the sites and diffusion paths identified from the MD simulations. Upper part: Sensitivities  $\psi(\mathcal{P}_{\star}^{\text{BV}}|\mathcal{P}_{\star})$ ; lower part: specificities  $\psi(\mathcal{P}_{\star}|\mathcal{P}_{\star}^{\text{BV}})$ .

	$\mathcal{P}_{\text{ex}}^{\text{BV}}$	$\mathcal{P}_{\text{cn}}^{\text{BV}}$	$\mathcal{P}_{\text{ex+cn}}^{\text{BV}}$
$\mathcal{P}_{\text{sites}}$	0.83	0.95	0.79
$\mathcal{P}_{\text{perc}}$	0.62	0.91	0.57
$\mathcal{P}_{\text{sites}}$	0.12	0.02	0.13
$\mathcal{P}_{\text{perc}}$	0.43	0.08	0.48

the space. The combined conditions (i-iii) reduce the accessible space to 8.3%, corresponding to an uncorrelated behavior. If conditions (ii-iv) are replaced by condition (v) in the limit  $d_{\text{th}} \rightarrow \infty$  the available space is restricted to 21.3% of the volume of the system (see also Fig. 6). One should expect that this accessible space entails the ionic sites and the diffusion path identified in sec. III.

To quantify the quality of agreement between the subsets  $\mathcal{P}_{\star}^{\text{BV}}$  ( $\mathcal{P}_{\star}^{\text{BV}} = \mathcal{P}_{\text{ex}}^{\text{BV}}$ ,  $\mathcal{P}_{\text{cn}}^{\text{BV}}$ , or  $\mathcal{P}_{\text{ex+cn}}^{\text{BV}}$ ) with the subsets  $\mathcal{P}_{\star}$  obtained from the MD simulations ( $\mathcal{P}_{\star} = \mathcal{P}_{\text{sites}}$  or  $\mathcal{P}_{\text{perc}}$ ), we define two quantities, the sensitivity and specificity. The sensitivity is the conditional probability  $\psi(\mathcal{P}_{\star}^{\text{BV}}|\mathcal{P}_{\star})$  that a cell belonging to one of the subsets identified in the MD simulations belongs to one of the subsets of the BV analysis. Conversely, the specificity of the BV analysis is quantified by calculating the conditional probabilities  $\psi(\mathcal{P}_{\star}|\mathcal{P}_{\star}^{\text{BV}})$ .<sup>41</sup>

Table IV summarizes the results. Let us in particular consider the case where conditions (i-iii) are applied (corresponding to  $\mathcal{P}_{\text{ex+cn}}^{\text{BV}}$ ). A high sensitivity of 79% is reached for the sites. However, from table III we see that the volume fraction of  $\mathcal{P}_{\text{ex+cn}}^{\text{BV}}$  (8.3%) is by a factor of about 6 larger than that of  $\mathcal{P}_{\text{sites}}$  (1.4%). Accordingly, the specificity  $\psi(\mathcal{P}_{\text{sites}}|\mathcal{P}_{\text{ex+cn}}^{\text{BV}}) = 13\%$  is rather low. The sensitivity for the diffusion path is 57% ( $\mathcal{P}_{\text{perc}}$ ). It is significantly lower than that for the sites, since the path contains regions with very low occupation probability (cf. Sec. III), which often violate the geometric constraints (i,ii).

The question is, whether the specificity can be improved without significant reduction in the sensitivity by applying condition (iv) in addition to (i-iii). The volume fraction  $v_{\text{BV}}$  of the BV path as a function of the threshold mismatch  $d_{\text{th}}$  is shown in Fig. 6 (solid line). For small  $d_{\text{th}}$ ,  $v_{\text{BV}}$  increases linearly and for  $d_{\text{th}} \gtrsim 0.3$  approaches the value 8.3% imposed by the constraints (i-iii). Figures 7a and b show how the sensitivity and specificity vary with  $d_{\text{th}}$  with respect to the sites and the diffusion path, respectively. The sensitivities in Figs. 7a,b start to saturate for  $d_{\text{th}} \gtrsim 0.2 - 0.3$ , a value in fair agreement with typical choices used in BV analyses of RMC models.<sup>42</sup> Close to  $d_{\text{th}} \simeq 0.1$ ,  $v_{\text{BV}} \simeq 5\%$  is by about 40% smaller than the saturation value 8.3% for  $d_{\text{th}} \rightarrow \infty$  (see Fig. 6). However, this reduction is not strong enough to

yield a significant improvement of the specificities. Even if one would take a large loss in the sensitivity by choosing  $d_{\text{th}}$  very small, the gain in the specificity remains low. In summary we find that the inclusion of criterion (iv) does not yield a substantial improvement and that the essential part of the obtained agreement is due to the geometric constraints (i,ii).

To find an optimal value for  $d_{\text{th}}$  with respect to both sensitivity and specificity, we use the maximum of Cohen's kappa value<sup>43</sup>. The kappa value for the sets  $\mathcal{A} = \mathcal{P}^{\text{BV}}(d)$  and  $\mathcal{B} = \mathcal{P}_*$  is defined by

$$\kappa = \frac{(p(\mathcal{A} \cap \mathcal{B}) + p(\bar{\mathcal{A}} \cap \bar{\mathcal{B}})) - (p(\mathcal{A})p(\mathcal{B}) + p(\bar{\mathcal{A}})p(\bar{\mathcal{B}}))}{1 - (p(\mathcal{A})p(\mathcal{B}) + p(\bar{\mathcal{A}})p(\bar{\mathcal{B}}))}, \quad (13)$$

where  $p(\cdot)$  denote the probabilities of the corresponding sets (for example,  $p(\mathcal{A} \cap \mathcal{B})$  is the probability that a cell belongs to both the sets  $\mathcal{A}$  and  $\mathcal{B}$ ). A value of  $\kappa = 1$  denotes complete agreement between the two sets, while  $\kappa = 0$  corresponds to a random overlap of the two sets (negative values indicate an anti-correlation). For the sites the maximum of  $\kappa$  occurs at  $d_{\text{th}} = 0.09$  and is only 25%. This is caused by the low specificity, which varies only slowly with  $d_{\text{th}}$ . At  $d_{\text{th}} = 0.09$  we find a specificity of 17%, while the sensitivity is 59%. For the path the maximum of  $\kappa$  occurs at  $d_{\text{th}} = 0.23$  and is 48%. The sensitivity and specificity attain values of 54% and 50% at this maximum. In summary, the quality of agreement for the path is promising, while that for the sites is not yet satisfactory.

The sensitivity for the diffusion path can however be improved and the influence of the BV sum mismatch increased by using condition (v) instead of conditions (ii-iv), i.e. by considering the path  $\mathcal{P}'_{\text{BV}}(d_{\text{th}})$ . For this path in comparison with  $\mathcal{P}_{\text{perc}}$  we plot in Fig. 8 the sensitivity and the specificity in dependence of  $d_{\text{th}}$  (see eq. (12)). For large  $d_{\text{th}}$ , the sensitivity reaches values up to 90%, which are significantly higher than the 57% in Fig. 7b. The specificity for small  $d_{\text{th}}$  has values comparable to that in Fig. 7b, and then decreases to smaller values for larger  $d_{\text{th}}$ . As a function of  $d_{\text{th}}$ ,  $\kappa$  reaches a maximum of 48% at  $d_{\text{th}} = 0.22$ . Further enhancements may be achieved by slight adjustments of the minimum distance  $R_{\text{LiSi}}$  or by replacing criterion (i) by a penalty function as well, which would mean that the oversimplifying hard sphere exclusion radius criteria (i,ii) may adversely affect the achievable level of agreement.

Finally, we test the potential of the BV method to identify sites (despite the low specificity). To this end we performed a cluster analysis with respect to  $d_{\text{th}}$ , analogous to the one carried out in sec. III with respect to  $\rho_{\text{cl}}$ . Different from the behavior found in Fig. 2, the number  $N_{\text{cl}}^{\text{BV}}$  of BV clusters shown in Fig. 9 is very large already for small  $d_{\text{th}}$  and then decreases rapidly due to coalescence of clusters. Accessible cells start to percolate at  $d_{\text{c}} = 0.09$ . The reason for this behavior is that the valence mismatch  $d(x)$  is a rather rapidly varying function. Already for small  $d_{\text{th}}$  there exists a large number of small

disconnected clusters that soon merge together to form a percolating cluster. While the majority of  $v_{\text{BV}}$  belongs to this percolation cluster the fluctuations in  $d(x)$  prevent  $N_{\text{cl}}^{\text{BV}}$  to assume comparatively small values for large  $d_{\text{th}}$ . Several hundred clusters are found for  $d_{\text{th}} \simeq 0.1$ . Almost all of these are very small: 80% consist of only a single cell and only 8 clusters contain more than 100 cells (i.e. are comparable to the size of sites). The percolation cluster includes 95% of  $v_{\text{BV}}(d_{\text{th}} = 0.1)$ . As a consequence the cluster analysis is not successful for identifying ionic sites with respect to  $d_{\text{th}}$ .<sup>44</sup>

It is interesting, however, that the BV analysis can provide a good estimate of the number of sites (not their location in space). It turns out to be useful to include the coordination number constraint (iii) in addition to the conditions (i,v) in this case. For varying mismatch threshold  $d_{\text{th}}$  the cells belonging to the corresponding path  $\mathcal{P}'_{\text{BV}}(d_{\text{th}})$  are filled row by row under the condition that two centers have a distance larger than the minimal Li-Li distance  $R_{\text{LiLi}} = 2.62$ . The number of sites found in this way is shown in Fig. 10 as a function of the mismatch threshold  $d_{\text{th}}$  (lower panel). For large  $d_{\text{th}}$ , it approaches the number of clusters found by the Hoshen/Kopelman analysis in Sect. III. On the other hand, we can take the estimated number of sites at the optimal bond valence mismatch  $d_{\text{th}} = 0.22$  given by the maximum of Cohen's  $\kappa$  value with respect to the sets  $\mathcal{P}_{\text{sites}}$  and  $\mathcal{P}'_{\text{BV}}(d_{\text{th}})$ . The result displayed in Fig. 8 yields 151 sites. This value is surprisingly close to the 148 sites found in Sec. III but studies of further systems are required to test whether such a prediction is generally possible.

In view of the success of the BV method to estimate the number of sites, we undertook further attempts to improve the level of agreement for the localization of the Li sites. If one distributes Li ions more randomly on the path  $\mathcal{P}'_{\text{BV}}(d_{\text{th}})$  with the same minimal distance constraint  $R_{\text{LiLi}} = 2.62 \text{ \AA}$ ,<sup>45</sup> instead of doing it row by row as described above, the positioning of centers of sites is no longer biased to the rim of the BV path. In this way, we obtain 165 BV clusters for  $d_{\text{th}} = 0.14$ . Considering now as BV sites the spheres with ion radius  $R_{\text{LiLi}}/2 = 1.31 \text{ \AA}$ , we found that 75% of these sites have at least one cell in common with one of the MD sites found in Sec. III. Still this is not enough for a reliable localization of Li sites.

## VI. SUMMARY AND PERSPECTIVES

We have identified sites and diffusion paths for the mobile Li ions in molecular dynamics simulations of a  $\text{Li}_2\text{SiO}_3$  glass. The identification was based on a cluster analysis of regions with high Li number density  $\rho(\mathbf{x})$ . For the clusters to be assigned to sites, we chose the condition that the total residence time of a Li ion on it (including intermediate escape to fringe regions) is ten times larger than the total hopping time to any of its neighboring clusters. Using this criterion, a very low concentration 2,8% of vacant sites was found. An attempt to identify

the diffusion path and sites by bond valence sums calculations was carried out. The comparison showed that the core of sites and parts of the diffusion path (up to about 50%) are captured. Conversely, the BV method was not suitable to distinguish between regions of high and low  $\rho(\mathbf{x})$ , and accordingly not suitable to determine the sites.

When dealing with the MD reference data of this work it proves to be necessary to adapt the BV parameters derived from experimental diffraction data to the MD force model. We showed that it is advantageous to optimize or replace the oversimplifying hard sphere exclusion radii for application of the BV analysis to the MD model. Moreover, an improvement of the BV analysis seems to be possible by adjusting the BV parameters  $r_0$  and  $\xi$  to the MD force model instead of only adjusting  $V_{id}$  to  $\bar{V}$ .

In searching for a powerful method to relate structural properties of the disordered network structure to transport properties of the mobile ions a further approach could be based on an effective potential  $U_{\text{eff}}(\mathbf{x}) \propto -k_B T \ln \rho(\mathbf{x})$ . Taking this effective potential one could perform a critical path analysis to determine the activation energy for the long-range ion mobility (see e.g. ref. 46). This approach would incorporate Coulomb interaction effects between the mobile ions in a mean field type approximation. Preliminary studies by us show that such Coulomb effects are important for the formation of the sites. With respect to the BV method we have also performed preliminary studies to evaluate the degree of correlation between  $U_{\text{eff}}(\mathbf{x})$  and the BV mismatch  $d(\mathbf{x})$  (or  $d'(\mathbf{x})$ ). It turned out that BV method cannot clearly distinguish between regions of high and low  $\rho(\mathbf{x})$  and accordingly it is not suitable to locate the sites. Besides

the described shortcomings of a particular choice of parameter values this is mainly caused by neglecting the long-range Li-Li Coulomb repulsions.

The precise decomposition of the ion trajectories into residence and transition parts described in Sec. III moreover may allow one to bridge the time scale gap between molecular dynamics and coarse-grained Monte-Carlo simulations. Given two neighboring sites, many transitions of mobile ions can be followed and the average transition rate calculated. The elementary rates for the possible transitions can then be used in a subsequent Monte-Carlo simulation. However, such procedure is not particularly useful if one is not able to take into account the temperature dependence of the elementary rates. One possibility is to use MD data at various high temperatures, and to try to calculate from them activation energies for the elementary rates (if these follow an Arrhenius type behavior). With less effort, one could use again the density  $\rho(\mathbf{x})$  and the effective potential derived from it to determine the energetics of a coarse-grained hopping model. Further investigations in this direction have to be undertaken in order to establish a working multi-scale modeling of these complex amorphous systems.

### Acknowledgments

Financial support to S. A. by the NUS ARF (R-284-000-029-112/133) and to the authors from TU Ilmenau by the HI-CONDELEC EU STREP project (NMP3-CT-2005-516975) is gratefully acknowledged.

- 
- \* Electronic address: philipp.maass@tu-ilmenau.de; URL: <http://www.tu-ilmenau.de/theophys2>
- <sup>1</sup> W. Dieterich and P. Maass, Chem. Phys. **284**, 439 (2002).
  - <sup>2</sup> H. Lammert, M. Kunow, and A. Heuer, Phys. Rev. Lett. **90** (2003) 215901.
  - <sup>3</sup> J. Habasaki and Y. Hiwatari, Phys. Rev. B **69**, 144207 (2004).
  - <sup>4</sup> M. Vogel, Phys. Rev. B **70** 094302 (2004).
  - <sup>5</sup> H. Lammert and A. Heuer, Phys. Rev. B **70**, 024204 (2004).
  - <sup>6</sup> A. Heuer, H. Lammert, and M. Kunow, Z. Phys. Chem. **218**, 1429-38 (2004).
  - <sup>7</sup> H. Lammert, A. Heuer, Phys. Rev. B **72**, 214202 (2005).
  - <sup>8</sup> J. Habasaki and K. L. Ngai, J. Chem. Phys. **122**, 214725 (2005).
  - <sup>9</sup> A. Mayer, J. Horbach, W. Kob, F. Kargl, and H. Schober, Phys. Rev. Lett. **93**, 027801 (2004); K. Binder, J. Horbach, A. Winkler, W. Kob, Ceram. Int. **31**, 713 (2005).
  - <sup>10</sup> We note that the vacancies are generated as defect structures in the glassy network, which becomes frozen below the glass transition. Accordingly, their number concentration does not change with temperature (it may be slightly affected by aging effects). The situation is thus different from that in crystalline systems, where the number concentration of vacancies is in general thermally activated.
  - <sup>11</sup> R. Peibst, St. Schott, and P. Maass, Phys. Rev. Lett. **95**, 115901 (2005); P. Maass and R. Peibst, J. Non-Cryst. Solids, in press.
  - <sup>12</sup> J. C. Dyre, J. Non-Cryst. Solids **324** (2003) 192.
  - <sup>13</sup> M. Kunow and A. Heuer, Phys. Chem. Chem. Phys. **7**, 2131 (2005).
  - <sup>14</sup> C. Karlsson, E. Zanghellini, J. Swenson, B. Roling, D. T. Bowron, L. Borjesson, Phys. Rev. B, **72**, 064206 (2005).
  - <sup>15</sup> S. Adams and J. Swenson, Phys. Rev. Lett. **84**, 4144 (2000).
  - <sup>16</sup> J. Swenson and S. Adams, Phys. Rev. Lett. **90**, 155507 (2003).
  - <sup>17</sup> A. Hall, S. Adams, and J. Swenson, Ionics **10**, 396 (2004).
  - <sup>18</sup> S. Adams and J. Swenson, J. Phys.: Condensed Matter **17**, 87 (2005).
  - <sup>19</sup> J. D. Garrett, J. E. Greedan, R. Faggiani, S. Carbotte, I. D. Brown, J. Solid State Chem. **42**, 183 (1982).
  - <sup>20</sup> I. D. Brown, *The Chemical Bond in Inorganic Chemistry – The Bond-Valence Model* (Oxford University Press, New York, 2002).
  - <sup>21</sup> S. Adams, *Bindungsvalenzmodelle für Struktur-Leitfähigkeits-Beziehungen in Festelektrolyten*, Habilitation thesis (in German), Göttingen 2000.
  - <sup>22</sup> S. Adams, Solid State Ionics **165**, 1351 (2000).



- <sup>23</sup> J. Habasaki and I. Okada, *Molecular Simulation* **9** 319-326 (1992).
- <sup>24</sup> S. Adams, Proceedings of the Asian Solid State Ionics Conference, ACSSI X, Kandy, Sri Lanka, 2006.
- <sup>25</sup> T. L. Gilbert, *J. Chem. Phys.* **49**, 2640 (1968).
- <sup>26</sup> Y. Ida, *Phys. Earth Planet. Inter.* **13**, 87 (1976).
- <sup>27</sup> J. Habasaki, I. Okada, and Y. Hiwatari, *J. Non-Cryst. Solids* **183** 12 (1995).
- <sup>28</sup> R. D. Banhatti and A. Heuer, *Phys. Chem. Chem. Phys.* **3** 5104 (2001).
- <sup>29</sup> A. Heuer, M. Kunow, M. Vogel, and R. D. Banhatti, *Phys. Chem. Chem. Phys.* **4** 3185- (2002).
- <sup>30</sup> The  $r^{-6}$  dependence can be motivated by the van-der-Waals interaction. However, since this term is used both for distances corresponding to covalent bonding as well as large distances, it in fact is not a van-der Waals interaction and often referred to as “dispersive interaction”. Nevertheless, the amplitude factors  $c_i$ ,  $c_j$  are usually assumed to scale with the polarizabilities. This gives reason to include this term here only for the large oxygen ions.
- <sup>31</sup> J. Hoshen and R. Kopelman, *Phys. Rev. B* **14**, 3438 (1976).
- <sup>32</sup> The total hopping and residence time, of course, have to be normalized with respect to the simulation time to give an intrinsic cluster property. Alternatively, we could have defined averaged (with respect to the number of events) hopping and residence times. In order to calculate the occupation probabilities in Fig. 4a we preferred to determine the total times.
- <sup>33</sup> This reentering mainly corresponds to a local non-activated ionic motion around a site on short time scales. It also includes rare (jump-like) events where a Li ions enters only the fringe of a neighboring site and returns without reaching its core. We note, the local motions cannot be simply accounted for by an oscillatory type of rattling motion in a potential minimum (see J. Habasaki, K. L. Ngai and Y. Hiwatari, *J. Chem. Phys.* **122**, 054507 (2005)).
- <sup>34</sup> Differences among possible definitions of ion sites are not relevant for our comparison of sites and paths derived from MD simulations with those derived from the BV method in the present work. This holds because the volume of the clusters being excluded is small. For other purposes, for example, if one wants to discuss the microscopic mechanism of jumps, it could be important to consider a more careful determination of the threshold value for the  $t_{\text{res}}$  to  $t_{\text{hop}}$  ratio (see, for example, the discussion in ref. 3).
- <sup>35</sup> A. Bunde and S. Havlin, in: A. Bunde and S. Havlin (Eds.), *Fractals and Disordered Systems*, 2nd ed., (Springer, Heidelberg, 1996).
- <sup>36</sup> L. Pauling, *The nature of chemical bond* (Cornell University Press, 1967).
- <sup>37</sup> G. Donnay and R. Allman, *Am. Mineral.* **55**, 1003 (1970).
- <sup>38</sup> <http://kristall.uni-mki.gwdg.de/softBV/>
- <sup>39</sup> S. Adams, *Acta Crystallogr. Sect. B* **57**, 278-287 (2001).
- <sup>40</sup> In other BV studies an additional “sign criterion” is often used in order to avoid an erroneous classification due to the limited cell resolution. In this case a cell is also marked as accessible if a Li ion at its center fails to fulfill requirement (iii), but on the other hand  $d(\mathbf{x})$  at one of the centers of the nearest neighboring cells has opposite sign. However, in our case the cell resolution is fine enough so that this problem plays no role for all relevant  $d_{\text{th}}$  considered in the subsequent analysis.
- <sup>41</sup> This definition of specificity deviates from the usual one, as it is, for example, often applied in medical studies. In such studies the specificity is given by the conditional probability  $\psi(\bar{\mathcal{P}}_{\star}^{\text{BV}}|\bar{\mathcal{P}}_{\star})$  with  $\bar{\mathcal{P}}_{\star}^{\text{BV}}$  and  $\bar{\mathcal{P}}_{\star}$  being the complements of  $\mathcal{P}_{\star}^{\text{BV}}$  and  $\mathcal{P}_{\star}$ , respectively. Both definitions are related by  $\psi(\mathcal{P}_{\star}|\mathcal{P}_{\star}^{\text{BV}}) = \psi(\mathcal{P}_{\star})\psi(\mathcal{P}_{\star}^{\text{BV}}|\mathcal{P}_{\star})/[\psi(\mathcal{P}_{\star})\psi(\mathcal{P}_{\star}^{\text{BV}}|\mathcal{P}_{\star}) + (1 - \psi(\mathcal{P}_{\star}))(1 - \psi(\bar{\mathcal{P}}_{\star}^{\text{BV}}|\bar{\mathcal{P}}_{\star}))]$ , where  $\psi(\mathcal{P}_{\star})$  is the probability that a cell belongs to  $\mathcal{P}_{\star}$  (i.e. equal to the volume fraction given in table III).
- <sup>42</sup> A. Hall, S. Adams, and S. Adams, preprint.
- <sup>43</sup> L. Fleiss, *Statistical methods for rates and proportions*, 2nd. ed. (Wiley & Sons, New York, 1981) pp. 212-236.
- <sup>44</sup> Following the method proposed in ref. 18 to consider edge-sharing cells as belonging to the same cluster and to use a higher  $s_{\text{min}} = 0.075$  in criterion (iii) to exclude strongly asymmetric coordinations, yields a slightly better separation of the pathway into clusters. In that case the number of clusters is reduced to a more plausible number 217, of which 61 contain only 1 cell for  $d_{\text{th}} = 0.14$  (where clusters are still well separated).
- <sup>45</sup> This can be done, for example, by using the standard MD algorithm SHAKE, see e.g. M. P. Allen and D. J. Tildesley, *Computer Simulation of Liquids* (Oxford University Press, New York, (1987)).
- <sup>46</sup> P. Maass, *J. Non-Cryst. Solids* **255**, 35 (1999).

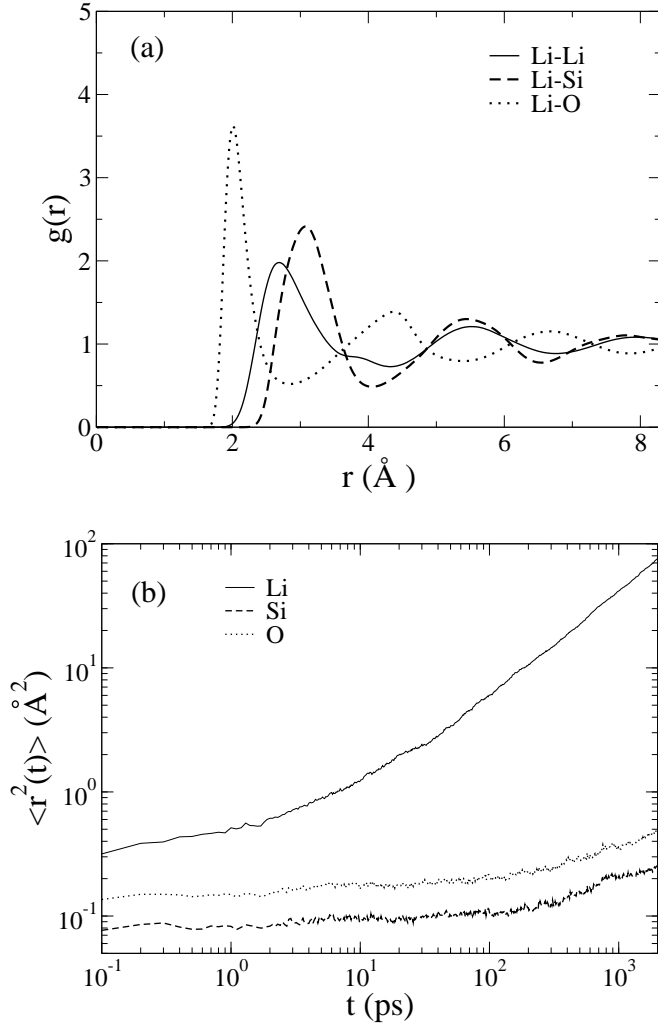


FIG. 1: (a) Pair correlation function of Li-Li, Li-Si and Li-O and (b) time-dependent mean square displacements of Li, O and Si ions at  $T = 700$  K.

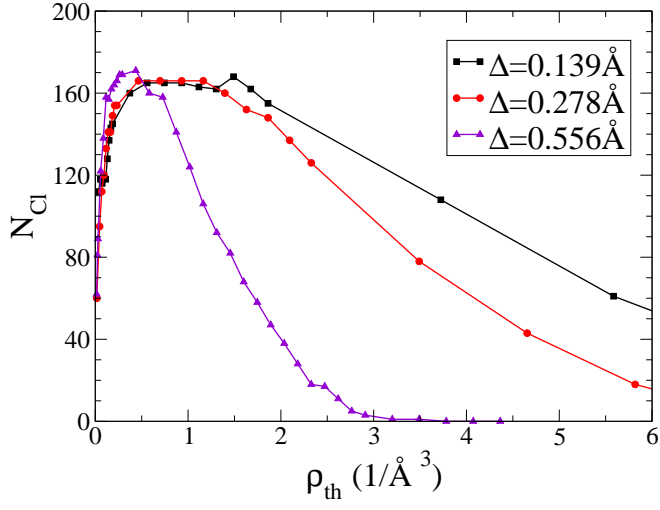


FIG. 2: Number of clusters  $N_{\text{cl}}$  in dependence of  $\rho_{\text{th}}$  for three different grid spacings  $\Delta$ . Note that the mean number density of Li ions is  $144/(16.68\text{\AA})^3 \simeq 0.031\text{\AA}^{-3}$  only, which in comparison with the relevant scale of  $\rho_{\text{th}}$  implies that the Li ions are strongly localized on the clusters.

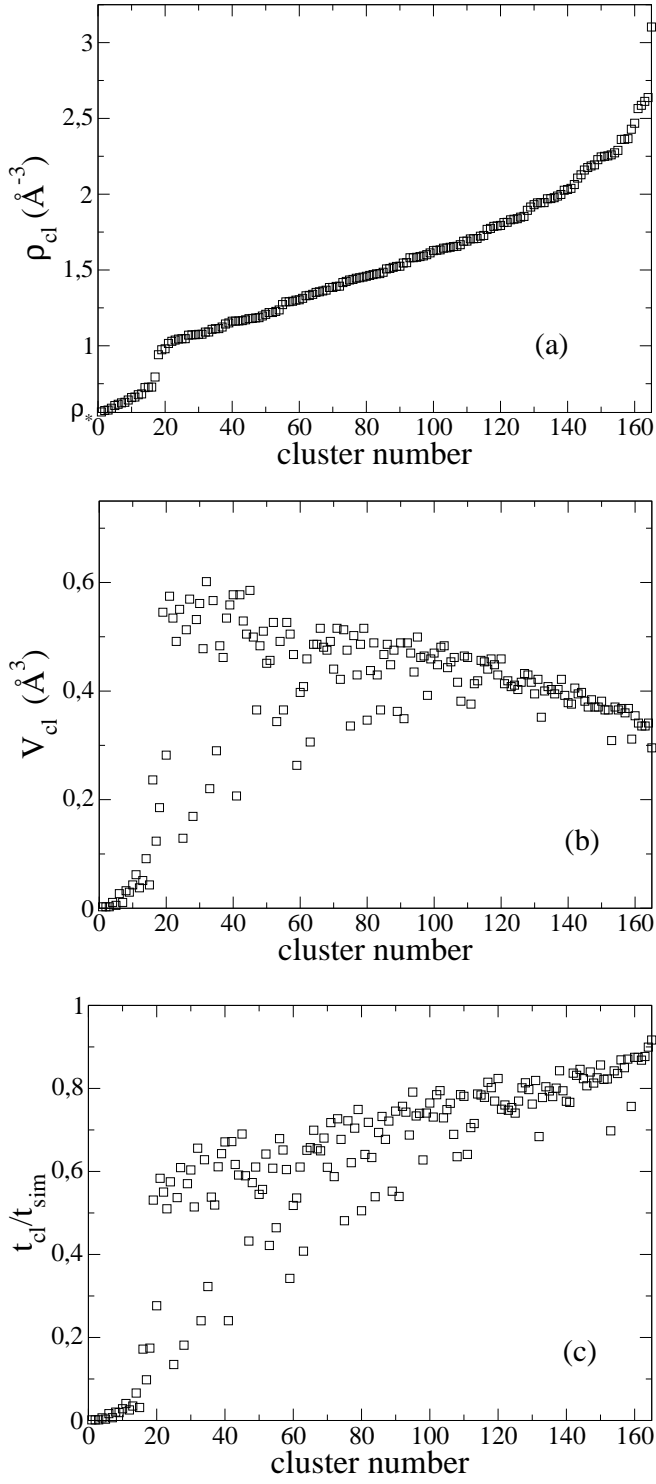


FIG. 3: (a) Mean number density  $\rho_{cl}$  of Li ions on the 165 clusters identified by the Hoshen-Kopelman algorithm; (b) Volume  $V_{cl}$  and (c) Li occupation probability  $t_{cl}/t_{sim}$  of the clusters. The clusters are sorted according to increasing  $\rho_{cl}$ .

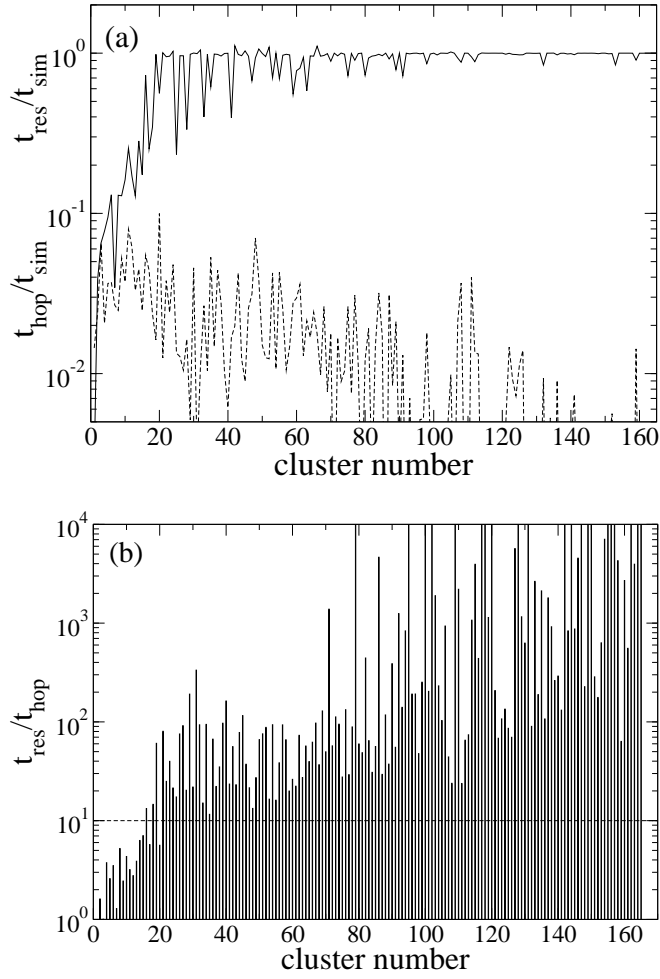


FIG. 4: (a) Total residence and hopping time normalized with respect to the simulation time  $t_{\text{sim}}$ , and (b) their ratio for the 165 clusters determined by the Hoshen-Kopelman algorithm. The dashed line marks the threshold above which clusters are identified as sites (cf. eq. 2).

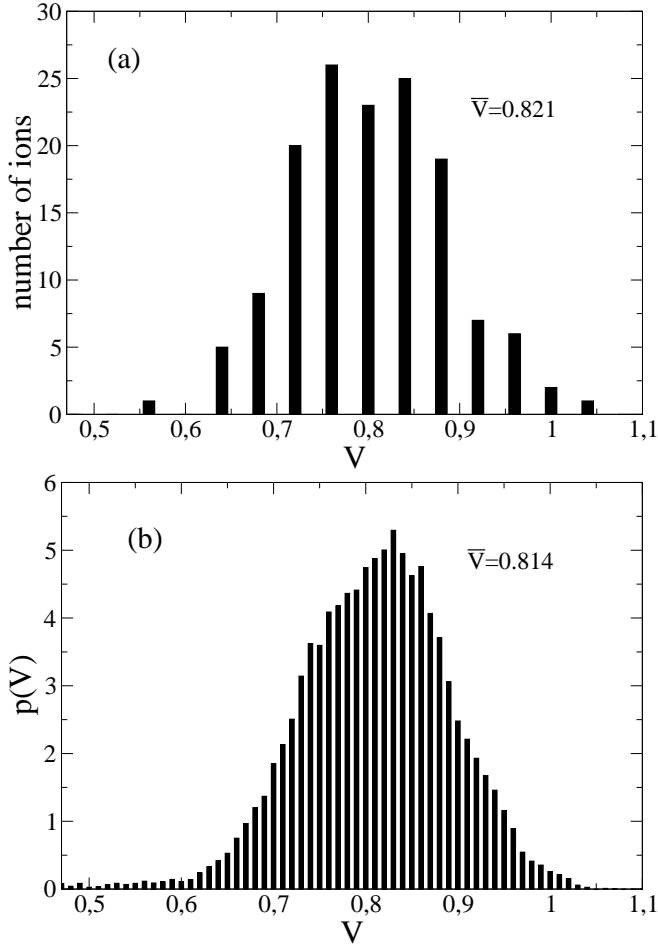


FIG. 5: (a) Histogram of of bond valence sums for an instantaneous configuration of the equilibrated  $\text{Li}_2\text{SiO}_3$  glass; (b) Probability density of bond valence sums with respect to the time-averaged structure of network forming O and Si ions.

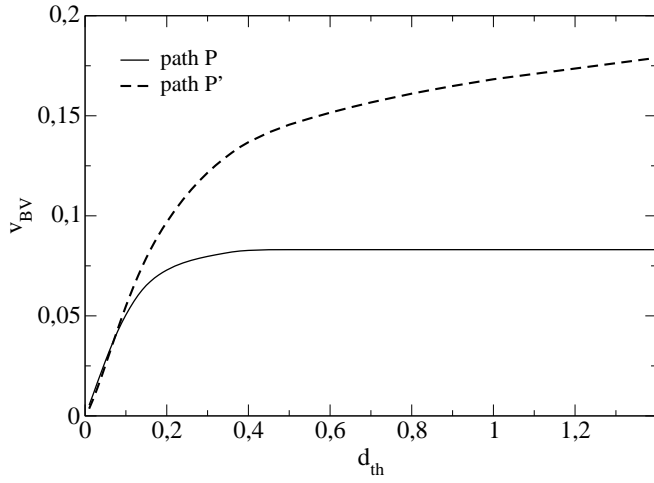


FIG. 6: Volume fraction  $v_{BV}$  of the BV path as a functions of the mismatch threshold  $d_{th}$ .

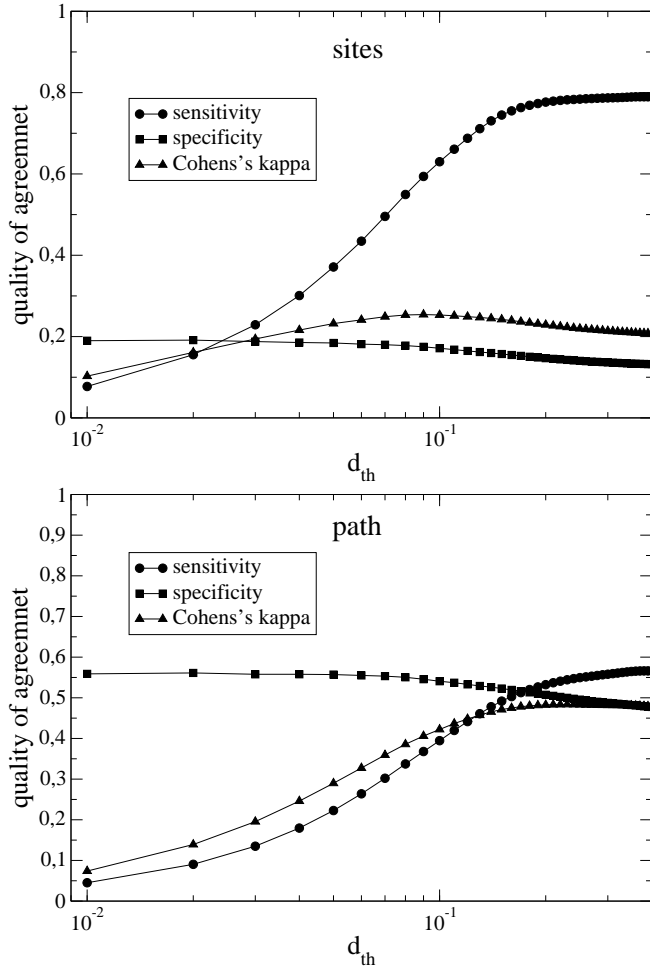


FIG. 7: Quality of agreement between (a) the subsets  $\mathcal{P}_{sites}$  and  $\mathcal{P}_{BV}(d_{th})$ , and (b) the subsets  $\mathcal{P}_{path}$  and  $\mathcal{P}_{BV}(d_{th})$ .

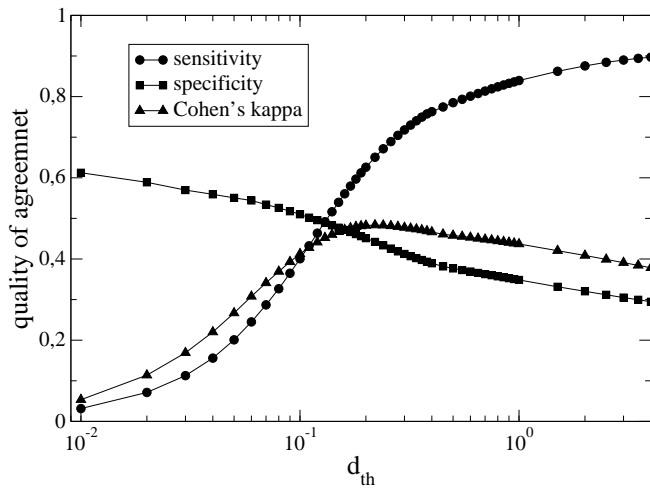


FIG. 8: Quality of agreement between the percolation path  $\mathcal{P}_{perc}$  and  $\mathcal{P}'_{BV}(d_{th})$  as a function of the BV mismatch threshold  $d_{th}$ .

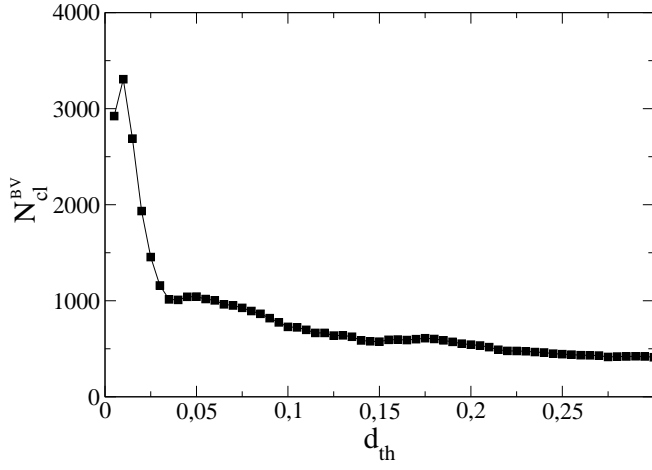


FIG. 9: Number of BV clusters as a function of the threshold mismatch  $d_{th}$ .

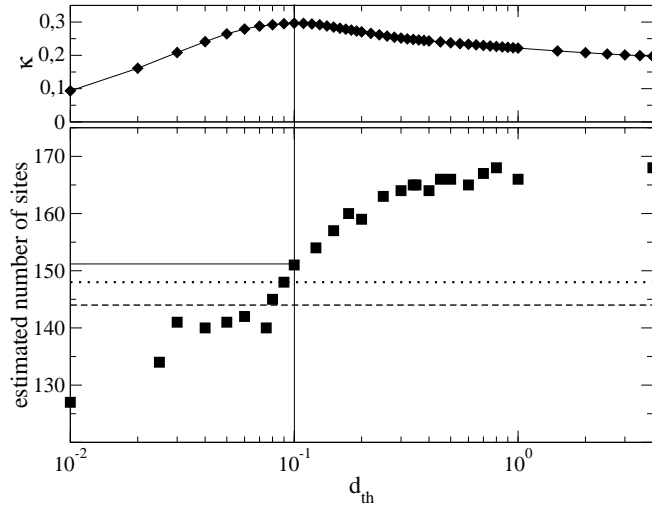


FIG. 10: Lower panel: Number of possible site centers on the BV path  $\mathcal{P}'_{BV}(d_{th})$  as determined by the “row-by-row algorithm” described in the text; Upper panel: Cohen’s kappa value for the path  $\mathcal{P}'_{BV}(d_{th})$  in comparison with  $\mathcal{P}_{perc}$  (re-drawn from Fig. 8). The number of estimated sites (151) at the optimal  $\kappa$  is indicated by the solid lines. The dashed line marks the number of Li ions (144) and the dotted line the number of sites (148) found in Sec. III.